Probing the Role of Mobility in the Collective Motion of Nonequilibrium Systems

Hongchuan Shen,[1] Peng Tan,[2,1,*] and Lei Xu[1,†]
[1]Department of Physics, The Chinese University of Hong Kong, Hong Kong, China
[2]Department of Physics, State Key Laboratory of Surface Physics, Fudan University, Shanghai 200433, China
(Received 19 June 2015; revised manuscript received 14 October 2015; published 29 January 2016)

By systematically varying the mobility of self-propelled particles in a 2D lattice, we experimentally study the influence of particle mobility on system's collective motion. Our system is intrinsically nonequilibrium due to the lack of energy equipartition. By constructing the covariance matrix of spatial fluctuations and solving for its eigenmodes, we obtain the collective motions of the system with various magnitudes. Interestingly, our structurally ordered nonequilibrium system exhibits properties almost identical to disordered glassy systems under thermal equilibrium: the modes with large overall motions are spatially correlated and quasilocalized while the modes with small collective motions are highly localized, resembling the low- and high-frequency modes in glass. More surprisingly, a peak similar to the boson peak forms in our nonequilibrium system as the number of mobile particles increases, revealing the possible origin of the boson peak from a dynamic aspect. We further illustrate that the spatially correlated large-movement modes can be produced by the cooperation of highly active particles above a threshold fraction, while the localized small-movement modes can be created by adding individual inactive particles. Our study clarifies the role of mobility in collective motions, and further suggests a promising possibility of extending the powerful mode analysis approach to nonequilibrium systems.

DOI: 10.1103/PhysRevLett.116.048302

Studying the collective motions or vibrational modes in solids is an important topic for condensed matter physics, as it plays an essential role in understanding the heat capacity, sound propagation, and thermal conductivity of solids. The powerful mode-analysis approach beautifully extracts the collective behaviors of an entire system from the motions of numerous individual particles. From these modes, deep insights of the system at different length and time scales can be obtained. In particular, this analysis has been widely applied to equilibrium systems, where "equilibrium" means a stable or metastable state that satisfies energy equipartition. However, the more general situation of nonequilibrium systems is largely unexplored. Using active-matter systems, we now tackle this important question at the single-particle level.

In equilibrium systems, energy equipartition simplifies the problem by ensuring that every particle and mode has the same energy, $\frac{1}{2}k_BT$. In crystals, the vibrational modes are plane waves and are excellently described by the Debye model. However, due to the structural disorders that break the translational invariance, the modes in disordered glassy systems are much more complex and interesting [1–16]. In particular, at low frequencies strong motions tend to concentrate at the defective soft spots, while the overall background is still like a plane wave [5,17–21]; this produces quasilocalized modes that play a crucial role in system rearrangements and relaxation [21–23]. The number density of these low-frequency modes also significantly exceeds the crystalline counterpart and forms the so-called "boson peak," whose origin is still under active debate [10,24–28]. As the frequency increases to the intermediate range, the modes become extended and uncorrelated. Once the high-frequency regime is reached, significant motions will concentrate only at very few rigid sites, which produces highly localized modes [20,29].

However, in nonequilibrium systems the important condition of energy equipartition breaks down. As a result, individual particles may have distinct kinetic energies or mobilities; thus, heterogeneity or "disorder" from a purely dynamic aspect can naturally arise. How does this special type of dynamic disorder affect the system? Is it similar to or different from the structural disorder, and can the two be understood in a unified picture? This fundamental issue underlies numerous nonequilibrium systems that do not satisfy energy equipartition. Clarifying this issue is also crucial for the important field of active-matter systems currently under intensive research, such as the cooperative behaviors of bacteria, birds, or fish within a large group, the collective motion of self-driven colloids, and the global movements and patterns of granular materials under external excitation [30–38]. However, due to the difficulty in controlling and adjusting the kinetic energy or mobility of every single particle, this fundamental puzzle remains an open question.

Using self-propelled active particles confined in a 2D square lattice, we systematically address this puzzle at the single-particle level. Our particles are identical metal spheres with $d = 13.00 \pm 0.01$ mm and $m = 9.915 \pm 0.005$ g (total mass of one sphere plus one motor). Each particle is connected to four nearest neighbors by identical springs

($k = 2.97 \pm 0.16$ N/m, $l_0 = 15.46 \pm 0.36$ mm); they form a square lattice as shown in Fig. 1(a). All springs are stretched to reach the lattice constant of 45.0 ± 1.5 mm, and the entire system contains $15 \times 15 = 225$ particles. To control the mobility at the single-particle level, under *every* particle we attach a small vibrating motor independently driven by external power input. Once turned on, motors will drive particles to move randomly around their equilibrium positions in 2D (see the Supplemental Movie [39]). Because the attractive interaction between particles is harmonic, the spatial fluctuations (renormalized by local variance) obey an excellent Gaussian distribution, as shown in Fig. 1(b). Clearly every particle has a well-defined equilibrium position, and the time-averaged deviation from it, $\langle \delta r_i \rangle = \langle \sqrt{\delta x_i^2 + \delta y_i^2} \rangle$, provides a good description for the mobility of each particle. Because of the distinct motor mobilities, $\langle \delta r_i \rangle$'s at different sites have a typical dispersion above 15%, which is much larger than the variations in lattice constant, particle mass, and interaction potential. Therefore, our system provides an ideal platform to probe the influence of mobility heterogeneity: both the structure and the interaction are set at their simplest situations, and only mobility varies significantly.

To understand the role of this mobility disorder in the collective motion, we construct the covariance matrix of spatial fluctuations and calculate its eigenmodes [19,38,40]. This particular principal component analysis on spatial fluctuations has great potential for extracting the system's collective movements: in equipartitioned equilibrium systems the eigenmodes are identical to the vibrational modes [38]. In nonequilibrium systems the eigenmodes are no longer the same as vibrational modes; however, they still reveal the systems collective motions at the single-particle level.

More specifically, we track the positions of all particles for 1250 frames (see the Supplemental Material for the influence of the frame number [39]) and we

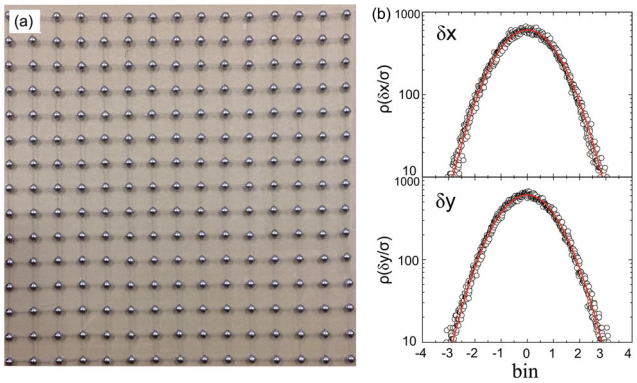

FIG. 1. (a) The image of our system. Identical metal spheres driven by independent motors are connected by springs to form a 2D square lattice. (b) The spatial fluctuations in both x and y directions for all particles and frames. The data for each particle are renormalized by the local variance σ. The red line is the standard Gaussian function.

construct the covariance matrix [19,38,40], $C_{i,j} = \langle [\boldsymbol{r}_i(t) - \langle \boldsymbol{r}_i(t) \rangle][\boldsymbol{r}_j(t) - \langle \boldsymbol{r}_j(t) \rangle] \rangle$, with $i, j = 1, \ldots, 2N_p$ running over the x and y coordinates of all particles and $\langle\rangle$ indicating time average over all frames. To eliminate the boundary effect, we only use the central $N_p = 11 \times 11 = 121$ particles, which results in $2N_p = 242$ eigenmodes. In equilibrium systems, these eigenmodes are identical to the vibrational modes, with the eigenvalue λ directly related to the vibrational frequency ω, $\omega \propto 1/\sqrt{\lambda}$ [17,38,40]. Analogous to ω, therefore, in our nonequilibrium system we define a dimensionless parameter, $\hat{\omega} \equiv \langle \delta\bar{r} \rangle / \sqrt{\lambda}$, which has the same λ dependence and is renormalized by the time-and-location-averaged displacement $\langle \delta\bar{r} \rangle$. Because of the lack of equipartition, our eigenmodes are no longer equivalent to vibrational modes and $\hat{\omega}$ is *not* the vibrational frequency, but these modes still indicate specific patterns of collective movements [see Fig. 2(a)], following which the system can achieve the overall displacement magnitude described by $\sqrt{\lambda}$ or $1/\hat{\omega}$ [37,38].

We show three typical modes at small, intermediate, and large $\hat{\omega}$ in Fig. 2(a): at small $\hat{\omega}$ polarization vectors exhibit large-scale correlations, at intermediate $\hat{\omega}$ they are rather random, and at high $\hat{\omega}$ motions localize on very few specific sites. These behaviors agree excellently with glassy systems under thermal equilibrium [17,38,40]. To quantify the spatial correlation, we plot the directional correlation function, $C(r) = \sum_{i,j=1}^{Np} \delta(r_{ij} - r) \hat{\mathbf{e}}_{\hat{\omega},i} \cdot \hat{\mathbf{e}}_{\hat{\omega},j} / \sum_{i,j=1}^{Np} \delta(r_{ij} - r)$ (here $\hat{\mathbf{e}}_{\hat{\omega},i}$ and $\hat{\mathbf{e}}_{\hat{\omega},j}$ are unit polarization vectors in mode $\hat{\omega}$), for the three modes in Fig. 2(b): it is apparent that large-scale correlation only exists at small $\hat{\omega}$, which is consistent with Fig. 2(a).

To illustrate the distribution of motion among different sites, we plot the participation ratio, $P(\hat{\omega}) = (\sum_i |\mathbf{e}_{\hat{\omega},i}|^2)^2 / (N_p \sum_i |\mathbf{e}_{\hat{\omega},i}|^4)$, in Fig. 2(c). A smaller P indicates a more localized mode and vice versa. Clearly, P starts relatively small at low $\hat{\omega}$, increases continuously to reach a peak at intermediate $\hat{\omega}$, and then decreases to rather small values at high $\hat{\omega}$. This trend in the P spectrum—from quasilocalized, to extended, and then to localized—again matches the equilibrium glassy systems very well. More careful inspection further reveals that at low $\hat{\omega}$ large motions concentrate on large-mobility particles, while at high $\hat{\omega}$ they localize at small-mobility particles. Comparing with previous studies on glassy systems, our large-mobility particles naturally correspond to the defective soft spots, and the small-mobility ones are analogous to the rigid spots [20]. This suggests that the mobility disorder has an influence similar to the structure and interaction disorder, raising the intriguing possibility of a unified understanding.

We illustrate the mode distribution of different-mobility samples with the spectrum analogous to the reduced density of states, $D(\hat{\omega})/\hat{\omega}$, in Fig. 3(a). To clarify the influence of particle mobility on the spectrum, we prepare sample A with a regular Gaussian $\langle \delta r_i \rangle$ distribution, sample B with extra small-mobility inactive particles, and samples

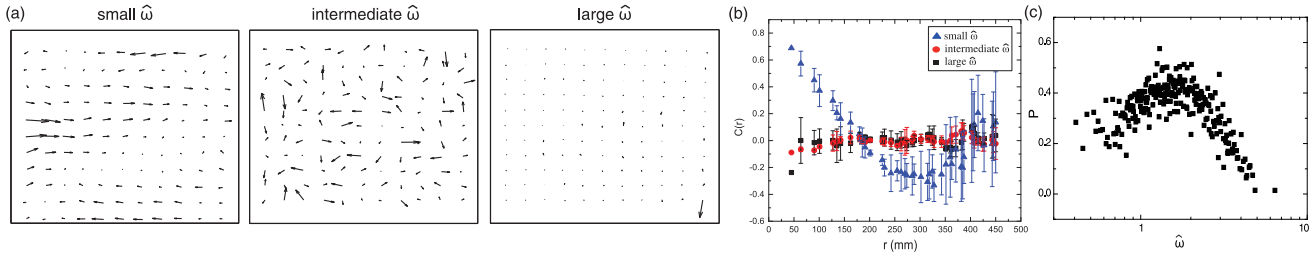

FIG. 2. (a) Three typical eigenmodes at small, intermediate, and large $\hat{\omega}$. (b) The spatial correlation function in direction for the three typical modes. (c) The participation ratio P of all the modes.

C and D with increasing amount of large-mobility active particles, as shown in Fig. 3(b). Interestingly, in sample A, $D(\hat{\omega})/\hat{\omega}$ is quite flat at low $\hat{\omega}$, which resembles the 2D crystal described by Debye model. Similarly, in sample B the low-$\hat{\omega}$ spectrum remains flat, indicating that adding inactive particles makes negligible influence. However, as more and more active particles are introduced into samples C and D, a low-$\hat{\omega}$ peak develops in an approach resembling the boson peak formation in glass. These data strongly suggest that the particles with large mobilities can produce extra low-$\hat{\omega}$ modes and cause the boson peak, while the inactive ones have no such effect.

To completely confirm this conclusion, we then tune the active particles in samples C and D back to normal activities; the peak then disappears, as shown in Fig. 3(c) and Supplemental Fig. 3 [39]. This result unambiguously verifies that the low-$\hat{\omega}$ peak is indeed caused by large-mobility particles. Comparing this with the boson peak formation due to defects in glass, our active particles naturally correspond to the defective *soft* spots, which are considered to be the origin of the boson peak [3]. With the mobility analysis, our study illustrates that the boson peak could originate with the mobility aspect, and suggests large mobility as the possible origin mechanism for the boson peak.

Clearly, the active particles can significantly affect the low-$\hat{\omega}$ modes. To obtain a complete picture, we further probe the importance of different-mobility particles throughout the entire $\hat{\omega}$ range. We pick three typical groups of particles with small, medium, and large mobilities respectively, and measure their relative importance in all eigenmodes. Each group contains 11 particles (9% of total N_p) and the data are shown in Fig. 3(d): as $\hat{\omega}$ increases, the importance of the large-mobility group changes from dominant to negligible, while the small-mobility group exhibits a completely opposite trend. Note that the 9% of large- and small-mobility particles account for almost 100% of the motion in the low- and high-$\hat{\omega}$ modes, respectively. By contrast, the medium-mobility group shows negligible importance at both low- and high-$\hat{\omega}$ regions, and only exhibits a weight comparable to the other two groups around the intermediate $\hat{\omega}$ indicated by a hatched area. This hatched region corresponds excellently to the peak position of the participation ratio in Fig. 2(c), as we naturally expect from the definition of extended modes.

To obtain an exact understanding on the role of particle mobility and further achieve desirable manipulation on the mode spectrum, we systematically introduce highly active or inactive particles into our system. Active particles all have mobilities above 240% of normal value, and inactive particles have mobilities below 45% of normal value. First, we replace normal particles with N_a highly active particles and plot the cumulative number of modes, $N(\hat{\omega})$, in Fig. 4(a). Significant change only occurs at low $\hat{\omega}$. More specifically, the curve with a small amount of active particles ($N_a = 5$, about 4%) does not show a noticeable deviation from the original $N_a = 0$ curve, while the curve

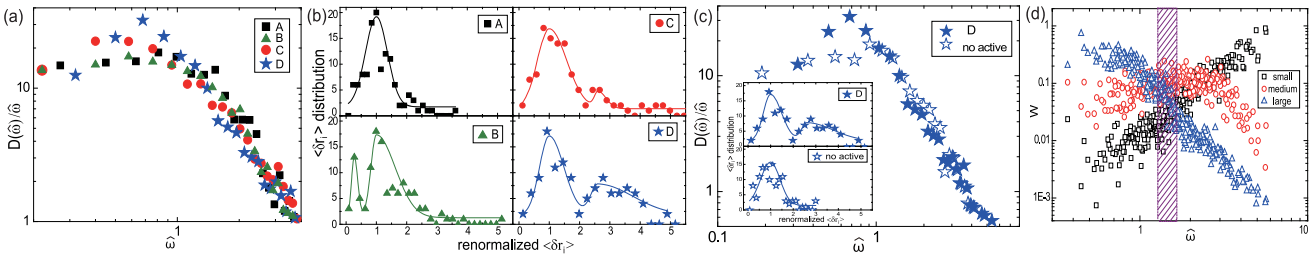

FIG. 3. (a) The $D(\hat{\omega})/\hat{\omega}$ spectra of four typical samples, A to D, demonstrate the formation of a low-$\hat{\omega}$ peak. (b) The distribution of time-averaged local displacement, $\langle \delta r_i \rangle$, for samples A to D. To achieve such distributions, the four samples are driven with different voltages: A (2.5 V), B (normally 2.5 V with 16.5% of 2 V), C (normally 2.5 V with 20.7% of 3.2 V), and D (normally 2.5 V with 20.7% of 3.2 V and 20.7% of 3.6 V). $\langle \delta r_i \rangle$'s are renormalized to make the main peak locate at 1. (c) Tuning the active particles in sample D back to normal activities eliminates the peak. Inset shows the $\langle \delta r_i \rangle$ distribution with and without active particles. (d) The relative importance of small-, medium-, and large-mobility groups throughout all $\hat{\omega}$. The hatched area where all groups are comparable corresponds to the peak in the participation ratio.

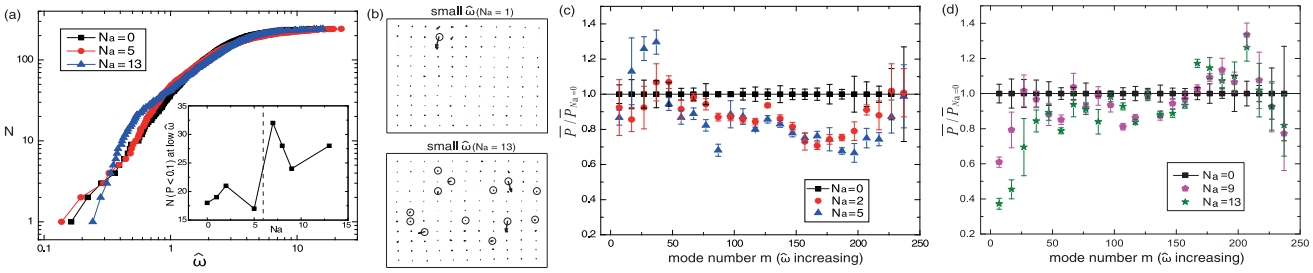

FIG. 4. (a) The variation in cumulative number of modes $N(\hat{\omega})$ as N_a active particles are added. Inset: the number of low-$\hat{\omega}$ quasilocalized modes ($P < 0.1$) versus N_a increases abruptly around the threshold value of $N_a = 6$ (i.e., 5%). (b) Large motions occur at the active-particle sites (labeled with circles) in the low-$\hat{\omega}$ modes. (c) and (d) compare the participation ratio in systems with and without active particles: panel (c) shows the situation of $N_a < 6$ and panel (d) the situation of $N_a > 6$.

with $N_a = 13$ (about 11%) shows a much sharper increase at the beginning, indicating the appearance of more low-$\hat{\omega}$ eigenmodes.

To obtain a quantitative understanding, we measure the number of low-$\hat{\omega}$ quasilocalized modes ($P < 0.1$) in systems with different N_a and plot it in the inset: an abrupt jump appears around $N_a = 6$ (i.e., 5%), as indicated by the dashed line. This threshold behavior implies that the low-$\hat{\omega}$ spectrum can only be significantly modified by adding *enough* mobile particles. Some typical low-$\hat{\omega}$ modes are directly visualized in Fig. 4(b), which confirms that large motions tend to occur at the highly active particles (labeled by circles). Although in the $N_a = 13$ image only a fraction of active particles exhibit large motions, other active particles experience similar large motions in the neighboring modes not shown here.

We further compare the participation ratio, P, for systems with different N_a against the original $N_a = 0$ system. To reduce random fluctuations, we average P over ten neighboring modes to obtain $\bar{P}$, and we calculate the ratio, $\bar{P}/\bar{P}_{Na=0}$, for all the modes. The values of $\bar{P}/\bar{P}_{Na=0}$ versus the mode number m (in the direction of increasing $\hat{\omega}$) are plotted in Figs. 4(c) and 4(d). Again we find two distinct behaviors: small amount of active particles do not produce systematic variations at low $\hat{\omega}$, although they seem to reduce the participation ratio at intermediate and high $\hat{\omega}$ [see Fig. 4(c)]; however, after N_a passes the threshold value, the participation ratio at low $\hat{\omega}$ reduces continuously with N_a [see Fig. 4(d)]. Together with the similar threshold behavior observed in Fig. 4(a), we conclude that the low-$\hat{\omega}$ spectrum cannot be modified by adding one or two active particles; instead, a threshold amount is required to create *new* spatially correlated low-$\hat{\omega}$ modes (not to just disturb existing ones, but to create new ones). A similar requirement may also hold for the generation of low-frequency modes in equilibrium glassy systems, although the exact threshold value may vary with specific conditions such as dimensionality, pressure, and temperature. The surprising appearance of the influence of small N_a's on the intermediate- and high-$\hat{\omega}$ modes in Fig. 4(c) is not understood and calls for further investigation.

Similarly, we can systematically replace normal particles with inactive particles. We again plot the cumulative number of modes, $N(\hat{\omega})$, for systems with N_i inactive particles in Fig. 5(a). Because the inactive particles mainly affect the large-$\hat{\omega}$ region, we use $1/\hat{\omega}$ as the x axis, which better stresses any change at large $\hat{\omega}$. As N_i increases, large-$\hat{\omega}$ modes are shifted to even higher $\hat{\omega}$. The quantitative measurements in the inset demonstrate that the number of high-$\hat{\omega}$ localized modes increases continuously with N_i and saturates at large N_i. This continuously increasing trend makes a sharp contrast to the abrupt jumping behavior for N_a in the inset of Fig. 4(a); the saturation is possibly due to the finite size of our system. Direct visualization of the

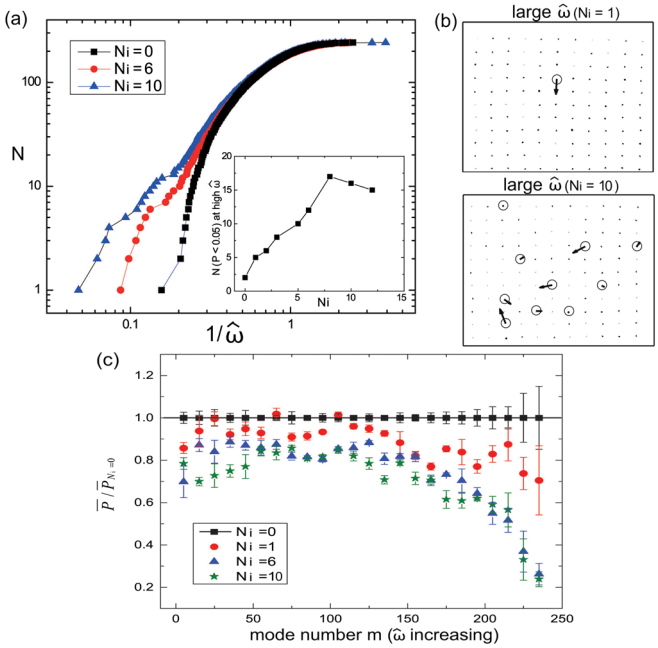

FIG. 5. (a) The cumulative number of modes $N(1/\hat{\omega})$ for different numbers of inactive particles. Inset: the number of high-$\hat{\omega}$ localized modes ($P < 0.05$) versus N_i. (b) Motions are concentrated at inactive particles (labeled with circles) in high-$\hat{\omega}$ modes. (c) As N_i increases, the participation ratio in the large-$\hat{\omega}$ region decreases significantly.

high-$\hat{\omega}$ localized modes are shown in Fig. 5(b): large motions tend to localize on the inactive-particle sites (labeled with circles) which confirms that the newly added inactive particles are responsible for these localized modes. For their influence on participation ratio, we again use the values in the original system, $\bar{P}_{Ni=0}$, as the control and plot the ratio $\bar{P}/\bar{P}_{Ni=0}$ in Fig. 5(c): as N_i increases, the ratio drops significantly at high $\hat{\omega}$, while no consistent trend is observed in the low-$\hat{\omega}$ region (see Supplemental Fig. 4 for more data [39]).

To summarize, the creation of spatially correlated low-$\hat{\omega}$ modes requires the collaboration of quite a few large-mobility particles, while the generation of localized high-$\hat{\omega}$ modes only needs individual inactive particles. The two distinct behaviors may also hold in glassy systems, and they may provide a potential guidance for the manipulation of mode spectrum in glass.

In conclusion, we have studied the role of particle mobility in the collective motions of 2D systems. Our results reveal that large- and small-mobility particles can significantly affect low- and high-$\hat{\omega}$ modes, respectively, which enables the spectrum to be effectively manipulated by adding active or inactive particles. Although our system is on an ordered square lattice, the difference in particle mobility causes collective motions very similar to disordered glassy systems. Therefore, the mobility disorder plays a similar role as the structural and potential disorder; this suggests a possible unification of all types of disorders. The quantities based on the time-averaged local displacement $\langle \delta r_i \rangle$ or local Debye-Waller factor can contain information from both the dynamic and the structural influences, and may provide a good order parameter for this unification. Indeed, such an order parameter has already demonstrated its great potential in the simulation of jammed spheres [41].

Moreover, we make further speculations on the comparison between equilibrium and nonequilibrium systems. With the knowledge of spring constant k, particle mass m, and system size, we can theoretically obtain the range of vibrational frequencies for our lattice as 9.75 to 34.62 Hz. By assuming that each mode roughly has the energy of $\frac{1}{2}k\langle \bar{\delta r} \rangle^2$, we can also obtain the frequency range from covariance matrix measurements, $\hat{\omega}\sqrt{k/m} \sim 3.6$ to 372.7 Hz. Note that this assumption is not strictly valid due to the lack of energy equipartition, and we make it only for the comparison with theoretical frequencies. It is apparent that the two results overlap reasonably well in the low-frequency regime, while at high frequencies the latter significantly exceeds the former; this indicates that equal partition might roughly hold for spatially correlated low-$\hat{\omega}$ modes, while serious breakdown only occurs at high frequencies. Similar to equilibrium systems, we also find correlations between real displacements and eigenmodes, as demonstrated in the projection plot in Supplemental Fig. 5 [39]. Our study on nonequilibrium systems suggests the possibility of extending the powerful mode-analysis approach from equilibrium systems to nonequilibrium active matter or even biological systems.

This project is supported by Hong Kong Research Grants Council under the projects of Early Career Schemes Grant No. CUHK404912 and General Research Fund Grant No. CUHK14303415; CUHK Faculty of Science under the Direct Grant No. 4053131 and Science Faculty Young Researcher Award 2014; and the National Natural Science Foundation of China No. 11504052.

*tanpeng@fudan.edu.cn
†xulei@phy.cuhk.edu.hk

[1] A. I. Chumakov, I. Sergueev, U. van Bürck, W. Schirmacher, T. Asthalter, R. Rüffer, O. Leupold, and W. Petry, Phys. Rev. Lett. **92**, 245508 (2004).
[2] M. Wyart, L. E. Silbert, S. R. Nagel, and T. A. Witten, Phys. Rev. E **72**, 051306 (2005).
[3] H. Shintani and H. Tanaka, Nat. Mater. **7**, 870 (2008).
[4] G. Monaco and V. M. Giordano, Proc. Natl. Acad. Sci. U.S.A. **106**, 3659 (2009).
[5] D. Kaya, N. Green, C. Maloney, and M. Islam, Science **329**, 656 (2010).
[6] E. M. Huisman and T. C. Lubensky, Phys. Rev. Lett. **106**, 088301 (2011).
[7] N. L. Green, D. Kaya, C. E. Maloney, and M. F. Islam, Phys. Rev. E **83**, 051404 (2011).
[8] V. Keppens, D. Mandrus, B. C. Sales, B. C. Chakoumakos, P. Dai, R. Coldea, M. B. Maple, D. A. Gajewski, E. J. Freeman, and S. Bennington, Nature (London) **395**, 876 (1998).
[9] R. O. Pohl, X. Liu, and E. Thompson, Rev. Mod. Phys. **74**, 991 (2002).
[10] H. Schober, J. Phys. Condens. Matter **16**, S2659 (2004).
[11] P. J. Yunker, K. Chen, Z. Zhang, and A. G. Yodh, Phys. Rev. Lett. **106**, 225503 (2011).
[12] Z. Zhang, N. Xu, D. T. Chen, P. Yunker, A. M. Alsayed, K. B. Aptowicz, P. Habdas, A. J. Liu, S. R. Nagel, and A. G. Yodh, Nature (London) **459**, 230 (2009).
[13] Z. Zhang, P. J. Yunker, P. Habdas, and A. G. Yodh, Phys. Rev. Lett. **107**, 208303 (2011).
[14] L. Wang and N. Xu, Soft Matter **9**, 2475 (2013).
[15] C. Zhao, K. Tian, and N. Xu, Phys. Rev. Lett. **106**, 125503 (2011).
[16] X. Wang, W. Zheng, L. Wang, and N. Xu, Phys. Rev. Lett. **114**, 035502 (2015).
[17] A. Ghosh, V. K. Chikkadi, P. Schall, J. Kurchan, and D. Bonn, Phys. Rev. Lett. **104**, 248305 (2010).
[18] N. Xu, V. Vitelli, A. Liu, and S. Nagel, Europhys. Lett. **90**, 56001 (2010).
[19] P. Tan, N. Xu, A. B. Schofield, and L. Xu, Phys. Rev. Lett. **108**, 095501 (2012).
[20] M. D. Gratale, P. J. Yunker, K. Chen, T. Still, K. B. Aptowicz, and A. G. Yodh, Phys. Rev. E **87**, 052301 (2013).
[21] K. Chen, T. Still, S. Schoenholz, K. B. Aptowicz, M. Schindler, A. C. Maggs, A. J. Liu, and A. G. Yodh, Phys. Rev. E **88**, 022315 (2013).

[22] K. Chen, M. L. Manning, P. J. Yunker, W. G. Ellenbroek, Z. Zhang, A. J. Liu, and A. G. Yodh, Phys. Rev. Lett. **107**, 108301 (2011).
[23] A. Ghosh, V. Chikkadi, P. Schall, and D. Bonn, Phys. Rev. Lett. **107**, 188303 (2011).
[24] M. I. Klinger, Phys. Rep. **94**, 183 (1983).
[25] W. Schirmacher, G. Diezemann, and C. Ganter, Phys. Rev. Lett. **81**, 136 (1998).
[26] T. Grigera, V. Martín-Mayor, G. Parisi, and P. Verrocchio, Nature (London) **422**, 289 (2003).
[27] G. Monaco and S. Mossa, Proc. Natl. Acad. Sci. U.S.A. **106**, 16907 (2009).
[28] A. I. Chumakov *et al.*, Phys. Rev. Lett. **106**, 225501 (2011).
[29] L. E. Silbert, A. J. Liu, and S. R. Nagel, Phys. Rev. E **79**, 021308 (2009).
[30] P. B. Umbanhowar, F. Melo, and H. L. Swinney, Nature (London) **382**, 793 (1996).
[31] T. E. Angelini, E. Hannezo, X. Trepat, M. Marquez, J. J. Fredberg, and D. A. Weitz, Proc. Natl. Acad. Sci. U.S.A. **108**, 4714 (2011).
[32] J. Bialké, T. Speck, and H. Löwen, Phys. Rev. Lett. **108**, 168301 (2012).
[33] S. Henkes, Y. Fily, and M. C. Marchetti, Phys. Rev. E **84**, 040301 (2011).
[34] D. Loi, S. Mossa, and L. F. Cugliandolo, Soft Matter **7**, 3726 (2011).
[35] G. S. Redner, M. F. Hagan, and A. Baskaran, Phys. Rev. Lett. **110**, 055701 (2013).
[36] J. Tailleur and M. E. Cates, Phys. Rev. Lett. **100**, 218103 (2008).
[37] C. Brito, O. Dauchot, G. Biroli, and J.-P. Bouchaud, Soft Matter **6**, 3013 (2010).
[38] S. Henkes, C. Brito, and O. Dauchot, Soft Matter **8**, 6092 (2012).
[39] See Supplemental Material at http://link.aps.org/supplemental/10.1103/PhysRevLett.116.048302 for Supplementary Movie and Information.
[40] K. Chen, W. G. Ellenbroek, Z. Zhang, D. T. N. Chen, P. J. Yunker, S. Henkes, C. Brito, O. Dauchot, W. van Saarloos, A. J. Liu, and A. G. Yodh, Phys. Rev. Lett. **105**, 025501 (2010).
[41] H. Tong and N. Xu, Phys. Rev. E **90**, 010401(R) (2014).